E3S Web of Conferences **730**, 01015 (2026) https://doi.org/10.1051/e3sconf/202673001015
Soft Soils 2026

Long-term settlement analysis of soft ground improved with the preloading method and centrifugal model tests for validation

Daisuke Niina[1*] and *Yoichi* Watabe[2]

[1] Civil Engineering Department, Toyo Construction Co., Ltd., Tokyo, Japan
[2] Division of Civil Engineering, Faculty of Engineering, Hokkaido University, Sapporo, Japan

Abstract. Preloading is widely used to reduce residual settlement in soft clays, but practical procedures for predicting long-term deformation after preload removal and reloading remain limited. This paper proposes a practical method based on the isotache concept, in which the consolidation yield pressure is uniquely related to the visco-plastic strain rate. The formulation for loading is extended to unloading and reloading so that complex load histories are treated within a single framework. Primary consolidation is solved using an axisymmetric consolidation equation, while time-dependent deformation is evaluated with an isotache constitutive model. The two calculations are updated sequentially in an uncoupled manner, avoiding a fully coupled implementation while maintaining computational efficiency. Centrifuge model tests were conducted in a cylindrical container with well-defined drainage and stress boundaries, and post-unloading behavior was monitored for over 48 h. The effects of removal timing (degree of consolidation), vertical drains, and initial stress level were examined parametrically. The tests showed elastic rebound and negative excess pore water pressure at unloading, followed by continued swelling or time-dependent resettlement after dissipation. The analysis qualitatively reproduced these responses, demonstrating applicability to moderate unloading conditions (OCR $\leq$ 1.4).

1 Introduction

The preloading technique is a representative ground-improvement method for soft clays, in which a temporary embankment load is applied to create an overconsolidated state before service. This increases soil strength and reduces residual settlement. For large facilities such as airport runways and container terminals, settlement may remain a long-term issue after inauguration, and rational prediction of settlement after preload removal is therefore an important design task. However, under non-monotonic load histories of loading–unloading–reloading, dissipation of excess pore water pressure associated with primary consolidation and time-dependent visco-plastic deformation may proceed simultaneously, making consistent prediction of post-unloading behavior difficult.

In engineering practice, primary consolidation is commonly evaluated using one-dimensional consolidation theory, and secondary compression is often treated as an additional settlement after the end of primary consolidation, such as by the C_α method [1]. In contrast, the isotache concept describes consolidation in a unified manner by a family of equal-strain-rate curves without separating primary and secondary consolidation in time; early foundations of this concept were presented by Šuklje [2], and related time-dependent compressibility concepts were further developed by Bjerrum [3]. The Japanese technical standards for port and harbor facilities adopt this framework [4]. However, a practical method that can evaluate such non-monotonic loading–unloading–reloading histories in a consistent manner has not yet been fully established.

To address this issue, this study proposes a practical analysis framework based on the isotache concept, in which loading, unloading, and reloading are treated within a single constitutive framework and the consolidation equation and constitutive update are solved sequentially in an uncoupled manner. The proposed method is examined through centrifuge model tests, which allow a self-weight stress field and controlled drainage boundaries to be reproduced in the model ground, enabling simultaneous observation of pore-pressure dissipation and surface settlement during unloading. In this study, post-unloading behavior is discussed mainly using representative measures that are less affected by measurement noise, namely surface settlement and layer-averaged excess pore water pressure, because layer-by-layer displacement after unloading was small and therefore more vulnerable to local measurement fluctuations.

The objectives of this study are to (i) organize the isotache-based constitutive relations so that loading, unloading, and reloading can be treated within a single framework, (ii) formulate a practical analysis method in which the consolidation equation and the constitutive update are solved sequentially in an uncoupled manner, and (iii) systematically characterize post-unloading long-term behavior (whether resettlement occurs and

* Corresponding author: niina-daisuke@toyo-const.co.jp

under what conditions) by centrifuge model tests that simulate preloading, and clarify the applicability and limitations of the proposed method.

2 Analysis method incorporating the isotache concept

2.1 Outline of the isotache model

2.1.1 Isotaches and consolidation yield pressure

In the isotache model, the consolidation yield pressure σ'^{p} is determined by the visco-plastic strain rate $\dot{\varepsilon}^{\mathrm{vp}}$. In the formulation by Watabe and Leroueil [5], the relationship is expressed as:

$$\ln[(\sigma'^{\mathrm{p}} - \sigma'^{\mathrm{pL}})/\sigma'^{\mathrm{pL}}] = c_1 + c_2 \ln \dot{\varepsilon}^{\mathrm{vp}} \quad (1)$$

where σ'^{pL} denotes the consolidation yield pressure in the limit as the visco-plastic strain rate approaches zero, and c_1 and c_2 are isotache parameters. Equation (1) determines which isotache (equal-strain-rate curve) the state lies on. A decrease in strain rate with time is interpreted as a transition of the state point to a slower isotache.

2.1.2 Limit compression curve

The volumetric strain (here denoted by the one-dimensional total strain ε) is decomposed into an elastic component ε^{e} and a visco-plastic component $\varepsilon^{\mathrm{vp}}$. The slopes corresponding to the compression index C_{c} and swelling index C_{s} are defined as:

$$\lambda_\varepsilon = 0.434 C_{\mathrm{c}}/(1 + e_0) \quad (2)$$

$$\kappa_\varepsilon = 0.434 C_{\mathrm{s}}/(1 + e_0) \quad (3)$$

where e_0 is the initial void ratio. In the isotache model of Watabe and Leroueil, the limit compression curve is defined as the compression curve obtained as the visco-plastic strain rate $\dot{\varepsilon}^{\mathrm{vp}}$ approaches zero. With this definition, visco-plastic strain does not develop indefinitely but converges over a sufficiently long time. The visco-plastic component $\varepsilon^{\mathrm{vp}}$ is updated sequentially so that it is consistent with both the state point and the associated strain rate. This framework enables primary and secondary consolidation to be treated continuously during loading, and also allows time-dependent deformation after unloading to be described as a movement of the state point.

Fig. 1 illustrates a conceptual extension of the isotache model to unloading and reloading. Immediately after unloading, negative excess pore water pressure is generated by undrained expansion. As this suction dissipates, the effective stress gradually decreases toward the post-unloading equilibrium state. Once excess pore water pressure becomes nearly zero, effective stress is approximately constant and subsequent displacement can be organized mainly as time-dependent deformation under constant stress. When reloading increases effective stress, time-dependent deformation can develop depending on the state. Thus, the isotache framework can systematically evaluate time-dependent deformation while accounting for load history.

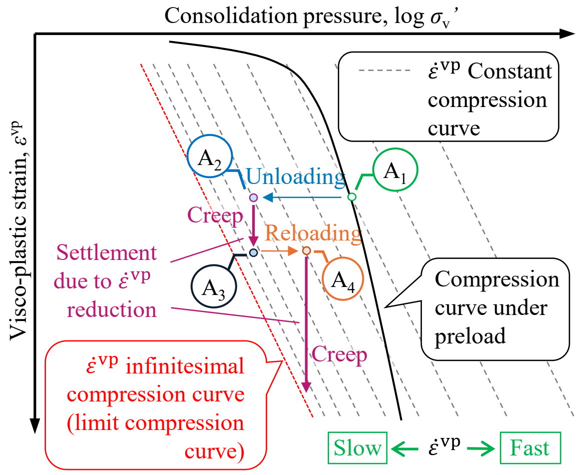

Fig. 1. Isotache model considering unloading and reloading.

2.2 Applicability limits of the proposed method

When the overconsolidation ratio (OCR) becomes large, viscous swelling may occur. Although a kinematic model referenced to the unloading point has been proposed to represent viscous swelling [6], viscous swelling (visco-plastic expansion) is not modeled in this study. Therefore, the proposed method becomes difficult to apply when the unloading magnitude is large and the post-unloading stress state shifts far to the left of the limit compression curve (Fig. 2).

The limit compression curve approximately corresponds to an overconsolidation ratio of OCR ≈ 1.4 relative to the initial consolidation yield pressure. Accordingly, large unloading conditions are excluded and applicability is limited to moderate unloading (OCR ≤ 1.4). Within this range, the proposed method reasonably reproduces elastic rebound after unloading, suction dissipation, and subsequent visco-plastic recompression.

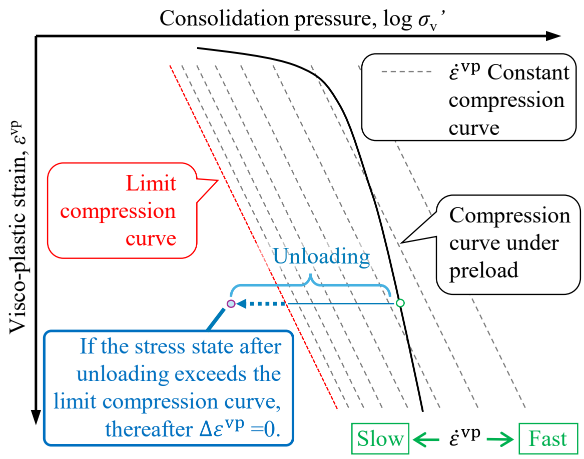

Fig. 2. Stress state after unloading.

2.3 Governing equations and numerical procedure

2.3.1 Consolidation equation

To account for cases where vertical drains are installed, an axisymmetric consolidation equation is adopted, considering vertical (z) and radial (r) drainage:

$$\frac{\partial u}{\partial t} = c_\mathrm{v}\frac{\partial^2 u}{\partial z^2} + c_\mathrm{h}\left(\frac{\partial^2 u}{\partial r^2} + \frac{1}{r}\frac{\partial u}{\partial r}\right) \qquad (4)$$

where u is excess pore water pressure, and c_v and c_h are consolidation coefficients in the vertical and horizontal directions, respectively. Radial drainage is considered when vertical drains are installed, whereas it is neglected (c_h = 0) in cases without vertical drains, leading to one-dimensional consolidation with single drainage.

2.3.2 Finite difference analysis

In the proposed method, Eq. (4) is first solved by a finite-difference scheme to obtain u at each time step, and the effective stress σ' is updated accordingly. Using σ'_{n+1} together with the state variables carried over from the previous step, σ'^{p}_{n+1}, $\dot{\varepsilon}^{vp}_{n+1}$, and ε^{vp}_{n+1} are solved iteratively so that the isotache relation and the strain decomposition are simultaneously satisfied (Fig. 3). The visco-plastic strain is updated as $\varepsilon^{vp}_{n+1} = \varepsilon^{vp}_{n} + \dot{\varepsilon}^{vp}_{n+1}\Delta t$, the total strain is then obtained from $\varepsilon_{n+1} = \kappa_\varepsilon \ln(\sigma'_{n+1}/\sigma'_0) + \varepsilon^{vp}_{n+1}$, and the total strain rate is evaluated as $\dot{\varepsilon}_{n+1} = (\varepsilon_{n+1} - \varepsilon_n)/\Delta t$. This procedure consists of a one-way sequential update of the consolidation equation, followed by effective-stress updating and constitutive updating, rather than a fully coupled implementation.

For thick layers where primary consolidation takes a long time, visco-plastic strain may develop during primary consolidation. After dissipation of excess pore water pressure, effective stress becomes nearly constant and long-term deformation is governed mainly by the update of $\dot{\varepsilon}^{\mathrm{vp}}$. Fig. 3 shows the analysis flowchart.

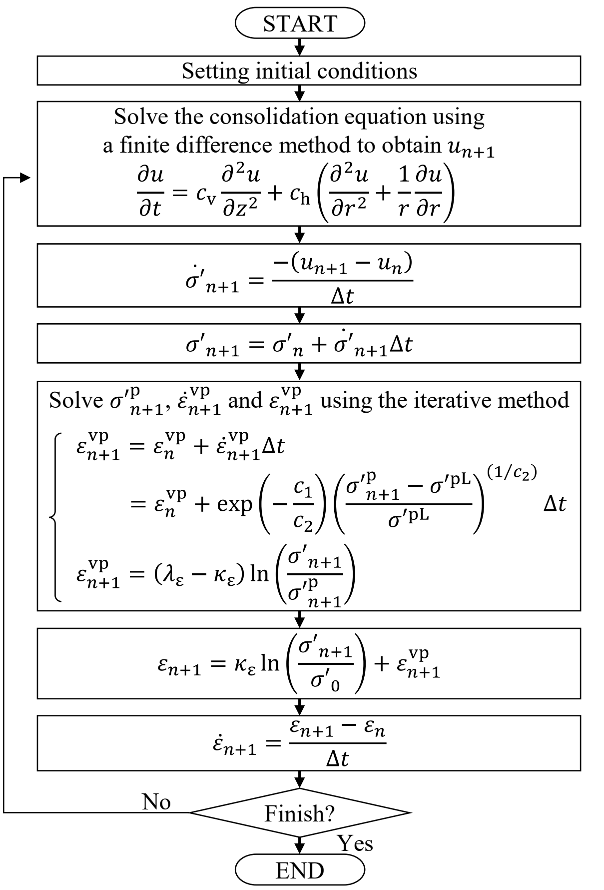

Fig. 3. Analysis flowchart.

2.3.3 Parameter setting

Parameters required for the analysis (c_v, c_h, C_c, C_s, γ', and e_0) can be obtained from standard laboratory tests. Isotache parameters ($\sigma'^{\mathrm{pL}}/\sigma'^{\mathrm{p0}}$, c_1, and c_2) can be determined from long-term consolidation tests, where σ'^{p0} denotes the consolidation yield pressure corresponding to a visco-plastic strain rate of 1×10^{-7} s^{-1}. However, to avoid case-by-case fitting and enhance practical usability, the standard values proposed by Watabe and Kaneko [7] based on worldwide long-term tests are adopted: $\sigma'^{\mathrm{pL}}/\sigma'^{\mathrm{p0}}$ = 0.7, c_1 = 0.935, and c_2 = 0.111.

3 Centrifuge model tests

3.1 Centrifuge apparatus

Centrifuge model testing can reproduce a prototype-equivalent stress field in a small model by applying a centrifugal acceleration Ng, and it is effective for investigating stress- and time-dependent phenomena such as consolidation and creep. Fig. 4 outlines the centrifuge test apparatus. A clay deposit 250 mm thick was prepared by self-weight consolidation in a steel

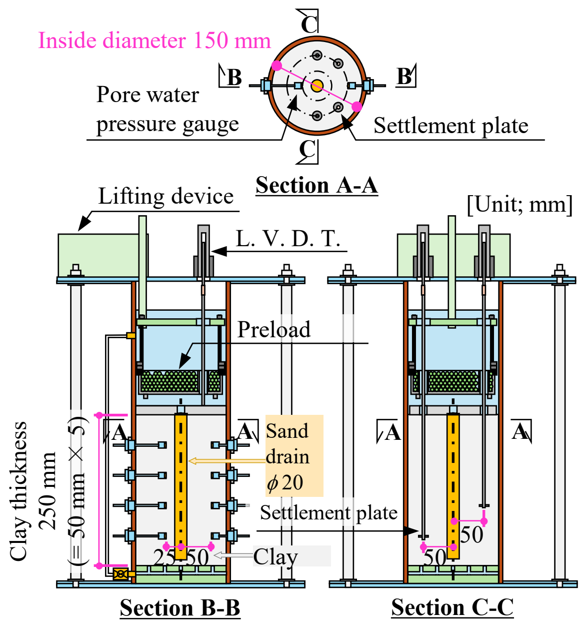

Fig. 4. Overview of the centrifuge model setup.

cylindrical container (150 mm in diameter and 500 mm in height). Excess pore water pressure was measured at several depths using miniature transducers, and vertical displacement was measured at the ground surface and at selected depths.

3.2 Test procedure

After self-weight consolidation, a preload of 50 kPa was applied. When a prescribed degree of consolidation was reached, the preload was instantaneously removed and post-unloading behavior was monitored for at least 48 h. The degree of consolidation was determined from the excess pore water pressure histories. Fig. 5 shows the test sequence.

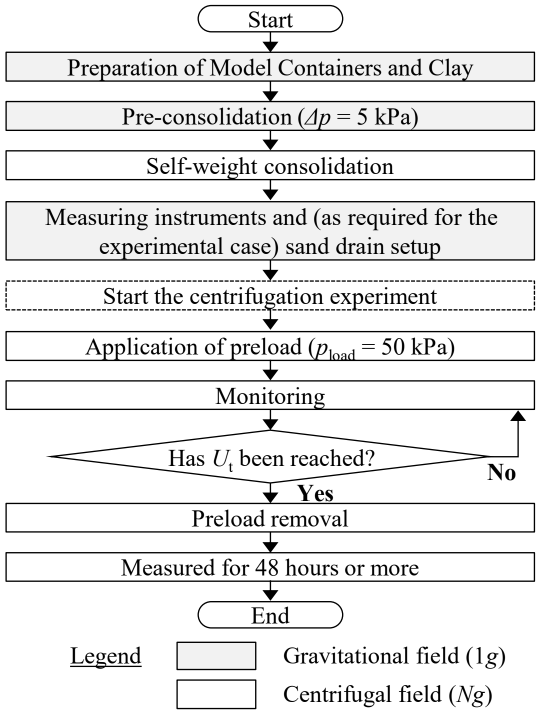

Fig. 5. Test flowchart.

3.3 Test cases

The test cases are tabulated in Table 1. The test matrix comprised 12 cases combining clay material (mixed clay or NSF kaolin), drainage condition (VD or ND), unloading timing ($U_t \approx 60\%$ or 90%), and centrifugal acceleration (50*g* or 25*g*).

3.3.1 Clay materials

To examine material effects, two clays were used: (i) a mixed clay prepared by mixing commercial NSF kaolin and Kibushi clay at a dry mass ratio of 6:4, and (ii) NSF kaolin. Because they differ in liquid limit, plasticity index, and consolidation coefficients, the influence of primary consolidation rate on post-unloading behavior can be compared. Table 2 summarizes the properties.

Table 1. Test cases (Case1–Case12).

Case	Clay	D. C.	U_t	C. A.
1	M. C.	VD	90%	50*g*
2	M. C.	VD	60%	50*g*
3	M. C.	ND	90%	50*g*
4	M. C.	ND	60%	50*g*
5	N. K.	VD	90%	50*g*
6	N. K.	VD	60%	50*g*
7	N. K.	ND	90%	50*g*
8	N. K.	ND	60%	50*g*
9	N. K.	VD	90%	25*g*
10	N. K.	VD	60%	25*g*
11	N. K.	ND	90%	25*g*
12	N. K.	ND	60%	25*g*

Abbreviations: M.C., mixed clay; N.K., NSF kaolin; D.C., drainage condition; C.A., centrifugal acceleration.

Table 2. Physical and consolidation properties of the clays.

Item	Unit	Mixed clay	NSF kaolin
Soil particle density, ρ_s	Mg/m^3	2.639	2.727
Liquid limit, w_L	%	57.5	46.7
Plastic limit, w_p	%	27.0	30.2
Plastic index, I_p		30.5	16.5
Compression index, C_c		0.42	0.33
Swelling index, C_s		0.071	0.042
Coefficient of consolidation, c_v	m^2/s	1.2×10^{-7}	1.2×10^{-6}

3.3.2 Drainage conditions (VD/ND)

Two drainage conditions were considered: a vertical-drain-improved condition (VD) and an unimproved condition (ND). For VD, radial drainage was idealized. For ND, single drainage from the ground surface was imposed by sealing the bottom boundary.

3.3.3 Degree of consolidation at unloading, U_t

The average degree of consolidation U_t is often used to describe the state at unloading. In this study, cases corresponding to a well-consolidated state ($U_t \approx 90\%$) and an insufficiently consolidated state ($U_t \approx 60\%$) were prepared to compare post-unloading behavior. However, especially under the ND condition, consolidation within the layer is necessarily nonuniform, so the average U_t does not uniquely represent the state of the entire deposit. Therefore, U_t is used here as a variable indicating the relative “earliness” or “lateness” of the removal time, rather than a strict threshold.

3.3.4 Initial effective stress level (centrifugal acceleration)

To investigate the effect of initial effective stress on long-term behavior, two centrifugal accelerations (50*g* and 25*g*) were applied. Self-weight consolidation was performed under the same acceleration so that the deposit was normally consolidated immediately before preload application.

3.4 Representative cases discussed in this paper

Although all test cases are listed in Table 1, only representative cases are discussed here. Case5 and Case6 (NSF kaolin, VD) are used as the primary comparison to isolate the effect of U_t, and Case7 (ND) is added for comparison of drainage condition. Detailed results for all cases are reported in [8]. The present paper does not aim to reproduce the full experimental dataset reported in [8], but rather to provide a focused interpretation of representative cases in order to clarify the governing mechanisms of post-unloading resettlement.

4 Experimental results

4.1 Behavior during unloading

Fig. 6 shows the time histories of excess pore water pressure (EPWP) and vertical displacement during unloading for Case5–7. Upon unloading, all cases exhibited a rapid recovery of vertical displacement (rebound) and a temporary negative excess pore water pressure. This stage corresponds to an elastic response due to undrained expansion under rapid stress release, followed by water intake, during which excess pore water pressure converges toward zero.

In this study, the time at which excess pore water pressure reaches approximately 0 kPa after the final load change is defined as EOP (end of primary consolidation) and used as a practical indicator of the onset of a stage dominated by viscous deformation.

4.2 Two patterns of long-term behavior after unloading

After excess pore water pressure converged near zero, the subsequent displacement fell into two patterns: continued swelling, or resettlement after initial swelling. The latter is the key target for model validation.

4.2.1 Cases without pronounced resettlement

In many cases where preload removal was relatively late ($U_t \approx 90\%$), post-unloading displacement progressed in the swelling direction and the swelling tendency continued at long times. In such cases, the post-dissipation effective-stress state tends to remain away from the limit compression curve (see Fig. 9), and the additional development of visco-plastic strain associated with isotache shifting is small.

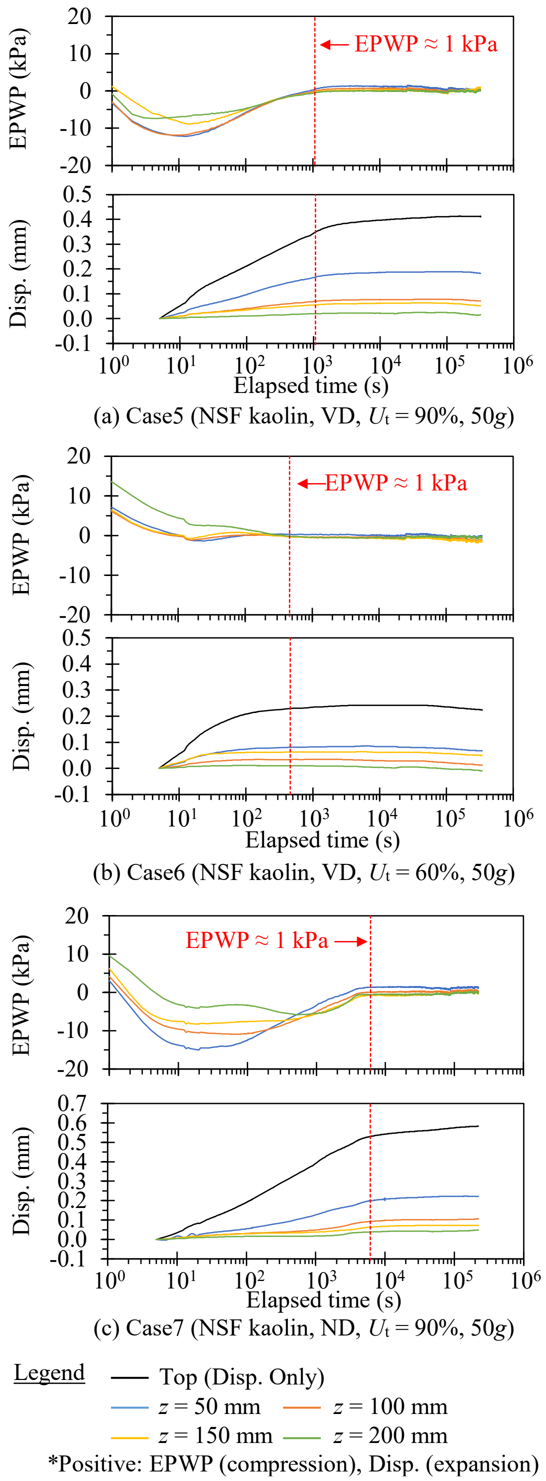

Fig. 6. Time histories of excess pore water pressure and vertical displacement during unloading (Case5–7).

4.2.2 Cases with resettlement

In contrast, some early-removal cases ($U_t \approx 60\%$) showed resettlement after the initial rebound and swelling. This paper focuses on VD cases, where drainage boundaries are clearer, and uses the comparison between Case5 and Case6 to isolate the effect of removal timing.

Differences in undissipated excess pore water pressure and strain rate at removal affect the post-dissipation effective stress state and hence the occurrence of resettlement. This mechanism is discussed in Section 6.1 using the total strain–effective stress relationship.

5 Reproduction analysis and validation of model applicability

5.1 Analytical model and boundary conditions

Fig. 7 shows the analytical model and boundary conditions used in the reproduction analyses. In the reproduction analyses, an axisymmetric model reflecting the geometry and drainage boundaries of the centrifuge tests is used. For VD, a radial drainage component is included. For ND, the bottom boundary is set as undrained to reproduce single drainage from the top surface. The analysis starts after completion of self-weight consolidation, and the clay is assumed to be normally consolidated at that time.

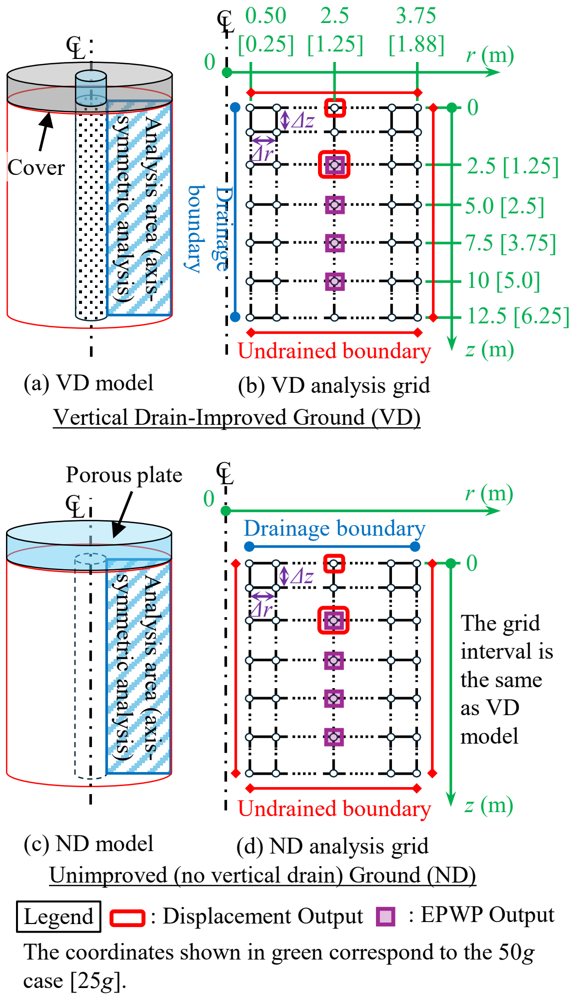

Fig. 7. Analytical model for reproduction analysis.

5.2 Parameters and adoption of standard values

The main parameters used in the reproduction analyses are tabulated in Table 3. Consolidation coefficients and compressibility parameters were identified by fitting to the experimental results and were distinguished between loading and unloading stages as needed. In contrast, isotache parameters were not fitted for each case; the same standard values were applied to all cases. This reduces the burden in parameter identification and provides guidance for practical application.

Table 3. Parameters used in reproduction analyses.

Item	Case5	Case6	Case7
Clay	N. K.	N. K.	N. K.
D. C.	VD	VD	ND
U_t	90%	60%	90%
γ' (kN/m^3)	7.24	7.24	7.24
C_c	0.25	0.29	0.22
C_s	0.011	0.010	0.015
c_{v_load} (m^2/s)	0	0	1.68×10^{-6}
c_{v_unload} (m^2/s)	0	0	1.68×10^{-5}
c_{h_load} (m^2/s)	2.50×10^{-6}	3.11×10^{-6}	0
c_{h_unload} (m^2/s)	6.94×10^{-6}	4.67×10^{-6}	0

Notes: For VD cases, c_v = 0 and for ND cases, c_h = 0, consistent with the adopted boundary conditions. Standard isotache parameters were used for all cases.

5.3 Treatment of similitude laws

In centrifuge modeling, similitude implies that the model dimensions are scaled by $1/N$, whereas effective stress and excess pore water pressure in the model are the same magnitude as in the prototype. The time scale for primary consolidation is shortened by $1/N^2$, while time-dependent deformation caused by soil skeleton viscosity corresponds to real time (1:1) and is essentially independent of centrifugal acceleration. Therefore, consistent treatment is required to compare consolidation and viscous deformation simultaneously.

In this study, reproduction analyses are performed at the prototype scale by multiplying c_v and c_h by N^2. The computed time and displacement are then converted to the model scale according to similitude. This allows consistent comparison while accounting for the different time scalings.

5.4 Comparison with centrifuge tests

Fig. 8 compares the reproduction analyses with the centrifuge test results. The settlement during loading and the dissipation process of excess pore water pressure are reproduced in reasonable agreement across differences in material, drainage condition, and centrifugal acceleration. During unloading, basic responses—elastic rebound and generation of suction—are also captured. Furthermore, for the resettlement observed in some $U_t \approx 60\%$ cases, the proposed method successfully captures the qualitative trend for displacement to turn to the settlement side after initial swelling.

On the other hand, for $U_t \approx 90\%$ cases where time-dependent swelling continues at long times, the analysis tends to show a plateau in displacement. This limitation is attributed to the simplification that viscous swelling is not modeled.

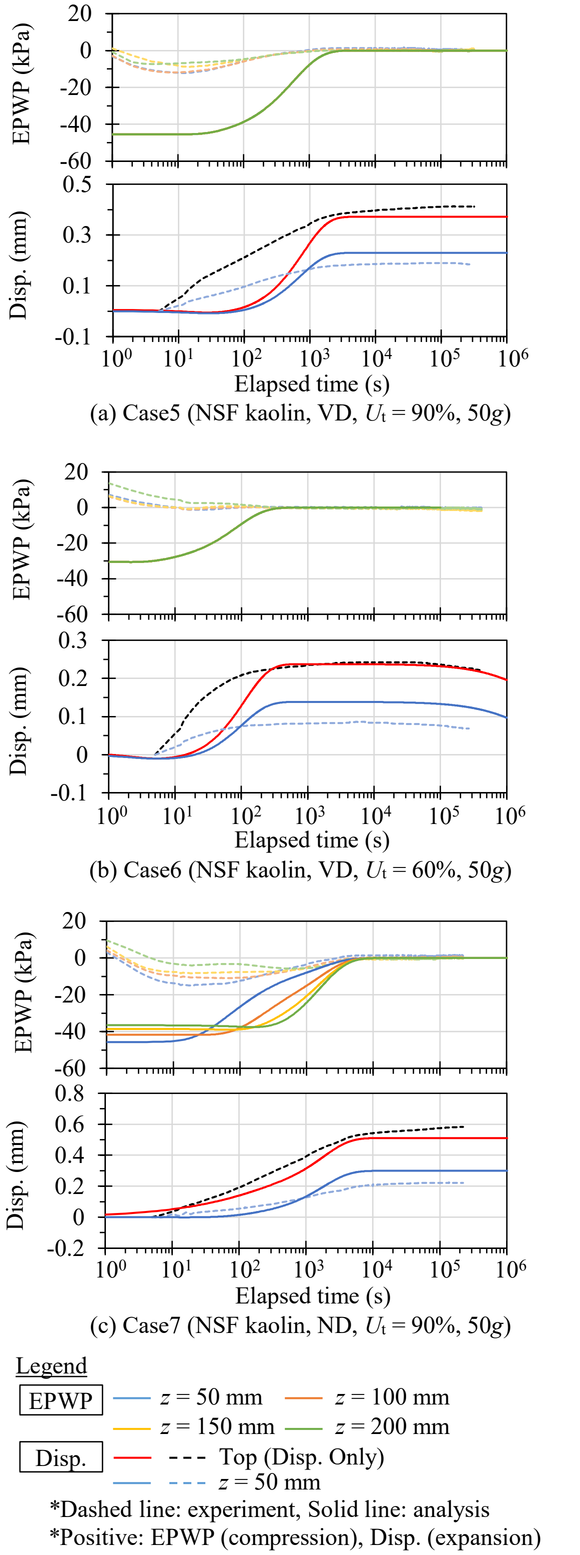

Fig. 8. Comparison between centrifuge tests and reproduction analyses.

6 Discussion

6.1 Influence of removal timing (U_t) on system response

The fundamental mechanism underlying the influence of removal timing is that the effective stress, the undissipated excess pore water pressure, and the strain rate at the time of removal are interrelated and together determine where the post-unloading state settles relative to the limit compression curve.

When removal is late, excess pore water pressure at unloading is small and the strain rate has already decreased. As schematically shown in Fig. 9, the post-dissipation state tends to remain away from the limit compression curve, and additional visco-plastic strain development due to isotache shifting is limited. In contrast, when unloading is performed early, the remaining excess pore water pressure is larger, and the effective stress acting after suction dissipation tends to approach the consolidation yield pressure. Under such conditions, the decrease in strain rate and the associated isotache shift lead to visco-plastic recompression (resettlement) after suction dissipation.

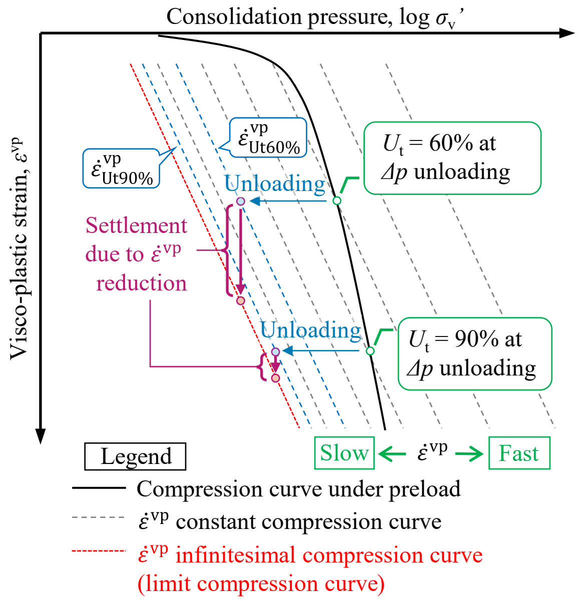

Fig. 9. Schematic effect of removal timing on the isotache response.

Fig. 9 schematically summarizes the influence of the degree of consolidation at removal on the post-unloading stress state and isotache shifting.

When removal is late, the state tends to lie away from the limit compression curve and resettlement is less likely. When removal is early, the state is more likely to return close to the limit compression curve, and visco-plastic recompression may develop after dissipation.

Because interpretation based only on settlement time histories can be ambiguous, representative cases were also organized by the total strain–consolidation pressure relationship. Fig. 10 was constructed by converting the measured ground-surface settlement to total vertical strain ($\varepsilon = s/H_0$, where s is surface settlement and H_0 is the initial clay thickness). The representative consolidation pressure σ'_v was evaluated at the mid-depth of the clay layer using the corresponding total stress and the layer-averaged excess pore water pressure, and the limit compression curve was plotted using the standard isotache parameters adopted in this study.

In Case 6, the representative path slightly crosses the limit compression curve; this is likely because the stress/strain pair in Fig. 10 is a simplified representative value (mid-depth stress and layer-averaged strain) whereas recompression is expected to be more pronounced at greater depth, together with measurement uncertainty and the use of non-calibrated standard parameters. For $U_t \approx 60\%$, the state point after

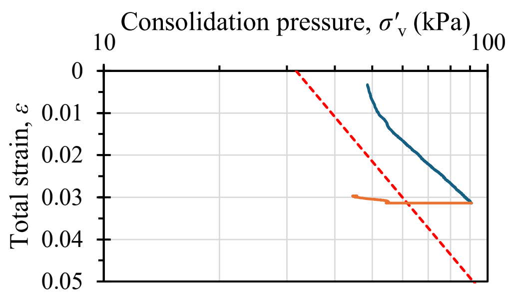

(a) Case5 (NSF kaolin, VD, $U_t = 90\%$, 50*g*)

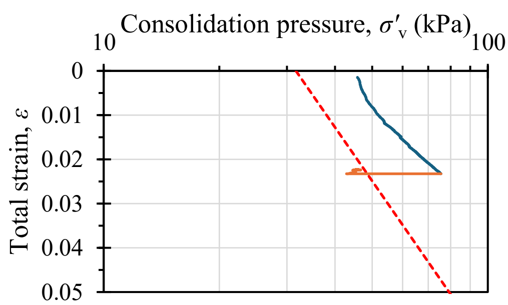

(b) Case6 (NSF kaolin, VD, $U_t = 60\%$, 50*g*)

Legend: Limit compression curve; Loading stage; Unloading stage

Fig. 10. Total strain–effective stress relationship (representative cases).

dissipation tends to return closer to the limit compression curve and recompression becomes apparent. For $U_t \approx 90\%$, the state point remains away from the limit compression curve and additional visco-plastic strain development is small, so swelling tends to continue.

6.2 Implications for practical design

In practical design, it is necessary to consider that settlement may continue even after excess pore water pressure has approached zero following preload removal. Within the applicability range (OCR $\leq$ 1.4), the proposed method can treat time-dependent deformation after dissipation continuously based on the isotache concept, in addition to evaluating primary consolidation. Unloading and reloading can be evaluated within a single constitutive framework, providing a rational prediction tool for moderate unloading conditions frequently encountered in practice.

7 Conclusions

This study establishes a practical isotache-based framework for evaluating long-term settlement behavior of preloaded soft clay under loading–unloading–reloading histories. The sequential uncoupled implementation enables efficient computation while retaining strain-rate-dependent behavior. Centrifuge experiments confirmed that removal timing governs post-unloading stress state evolution and the emergence of visco-plastic recompression. Within the moderate unloading range (OCR $\leq$ 1.4), the proposed method provides a rational and practical prediction tool. Extension to large unloading conditions incorporating viscous swelling remains a subject for future refinement.

References

1. G. Mesri, Y. K. Choi, Settlement analysis of embankments on soft clays, J. Geotech. Eng. ASCE, **111**(4), pp. 441-464 (1985). https://doi.org/10.1061/(ASCE)0733-9410(1985)111:4(441)
2. L. Šuklje, The analysis of the consolidation process by the isotaches method, Proc. 4th Int. Conf. Soil Mech. Found. Engng, London, **1**, pp. 200-206 (1957).
3. L. Bjerrum, Problems of soil mechanics and construction on soft clays and structurally unstable soils (collapsible, expansive and others), Proc. 8th Int. Conf. Soil Mech. Found. Engng, Moscow, **3**, pp. 111-159 (1973).
4. The Overseas Coastal Area Development Institute of Japan, Technical standards and commentaries for port and harbour facilities in Japan, pp. 333-336 (2025).
5. Y. Watabe, S. Leroueil, Modeling and implementation of the isotache concept for long-term consolidation behavior, Int. J. Geomech., **15**(5), A4014006 (2015). https://doi.org/10.1061/(ASCE)GM.1943-5622.0000270
6. Z. Fan, Y. Watabe, Experimental study for modeling unloading swelling behavior of Ariake clay, Soils and Foundations, **65**(3), 101594 (2025). https://doi.org/10.1016/j.sandf.2025.101594
7. Y. Watabe, T. Kaneko, Interpretation of long-term consolidation behavior of worldwide clays on the basis of the isotache concept, Rep. Port Airpt. Res. Inst., **54**(1), pp. 3-30 (2015) (in Japanese).
8. D. Niina, Y. Watabe, A practical isotache model approach for long-term settlement prediction of preload improved soft clay, Jpn. J. JSCE, **82**(1), 25-00196 (2026) (in Japanese). https://doi.org/10.2208/jscejj.25-00196